



ARTICLE

The aldose reductase inhibitor epalrestat exerts nephritic protection on diabetic nephropathy in db/db mice through metabolic modulation

Jun He¹, Hao-xue Gao¹, Na Yang¹, Xiao-dong Zhu², Run-bin Sun¹, Yuan Xie¹, Cai-hong Zeng², Jing-wei Zhang¹, Jian-kun Wang¹, Fei Ding³, Ji-ye Aa¹ and Guang-ji Wang¹

Epalrestat is an inhibitor of aldose reductase in the polyol pathway and is used for the management of diabetic neuropathy clinically. Our pilot experiments and accumulated evidences showed that epalrestat inhibited polyol pathway and reduced sorbitol production, and suggested the potential renal protection effects of epalrestat on diabetic nephropathy (DN). To evaluate the protective effect of epalrestat, the *db/db* mice were used and exposed to epalrestat for 8 weeks, both the physiopathological condition and function of kidney were examined. For the first time, we showed that epalrestat markedly reduced albuminuria and alleviated the podocyte foot process fusion and interstitial fibrosis of *db/db* mice. Metabolomics was employed, and metabolites in the plasma, renal cortex, and urine were profiled using a gas chromatography-mass spectrometry (GC/MS)-based metabolomic platform. We observed an elevation of sorbitol and fructose, and a decrease of myo-inositol in the renal cortex of *db/db* mice. Epalrestat reversed the renal accumulation of the polyol pathway metabolites of sorbitol and fructose, and increased myo-inositol level. Moreover, the upregulation of aldose reductase, fibronectin, collagen III, and TGF- β 1 in renal cortex of *db/db* mice was downregulated by epalrestat. The data suggested that epalrestat has protective effects on DN, and the inhibition of aldose reductase and the modulation of polyol pathway in nephritic cells be a potentially therapeutic strategy for DN.

Keywords: diabetes; diabetic nephropathy; polyol pathway; metabolomics; aldose reductase

Acta Pharmacologica Sinica (2019) 40:86–97; <https://doi.org/10.1038/s41401-018-0043-5>

INTRODUCTION

Diabetic nephropathy (DN) is a leading cause of end-stage renal disease and is considered a common microvascular complication of diabetic mellitus, with a high risk of atherosclerotic disease. Although the development and pathogenesis of DN remain unclear, previous studies have shown that the pathogenesis of DN is complex and involves multiple factors, including a markedly increased number of advanced glycation end (AGE) products, enhanced activity of protein kinase C, altered expression of cyclin-dependent kinases, and the activation of aldose reductase (AR) [1, 2]. AR (EC 1.1.1.21) was first discovered by Hers [3], and is currently accepted as one of the key mechanisms primarily responsible for the pathogenesis of diabetic complications [4, 5]. AR is the rate-controlling enzyme in the polyol pathway that catalyzes the reduction of glucose to sorbitol. It is proposed that excessive intracellular sorbitol produced by AR and fructose accumulates in cells and is difficult to diffuse across cell membranes [6]. Subsequently, the elevated sorbitol and fructose, along with the high level of glucose, markedly enhance osmotic stress inside cells, which eventually leads to a discharge of myo-inositol, one of the osmotic regulators, and finally diabetic cataract complication [7, 8]. Thus, AR provides a potential target for the design of drugs,

and the inhibition of AR has been an alternative approach for the prevention and treatment of diabetic complications, primarily diabetic neuropathy [9, 10].

Epalrestat, a post-market aldose reductase inhibitor (ARI) in Bangladesh, India, and China, is one of the most common ARIs for patients who suffer from diabetes mellitus [11]. As AR is the rate-controlling enzyme in the polyol pathway, epalrestat can significantly inhibit AR and downregulate polyol metabolites (such as sorbitol and fructose) to alleviate osmotic stress [1]. Except for diabetes neuropathy, recent accumulative evidence has suggested the potential application of ARIs for renal protection in DN [12, 13]. Li et al. [14] observed significant depletion of myo-inositol in the renal cortex of diabetic kidneys in *db/db* mice, which is observed in other animal models [15, 16]. It has been suggested that the activation of the polyol pathway and AR caused elevated sorbitol levels, osmotic stress of renal cells, and depletion of myo-inositol. We presumed that the osmotic damage caused by sorbitol accumulation and the depletion of myo-inositol was one of the confounding factors primarily contributing to renal dysfunction. Modulation of the polyol pathway and AR has a potential clinical benefit on the homeostasis of renal physiology in DN patients clinically [17].

¹Key Laboratory of Drug Metabolism and Pharmacokinetics, State Key Laboratory of Natural Medicines, China Pharmaceutical University, 210009 Nanjing, China; ²Research Institute of Nephrology of PLA, Jinling Hospital, 210002 Nanjing, China and ³Nanjing Hailing Pharmaceutical Co. Ltd., Yangzi River Pharmaceutical Group, Co. Ltd., 210049 Nanjing, China

Correspondence: Ji-ye Aa (jiyea@cpu.edu.cn) or Guang-ji Wang (guangjiwang@hotmail.com)

Received: 10 January 2018 Accepted: 17 April 2018

Published online: 21 June 2018

Recently, our pilot experiments in *db/db* mice showed that epalrestat alleviated renal pathology and reduced urinary excretion of albumin, indicating a potential effect of epalrestat on DN. To confirm the pharmacodynamic effects of epalrestat and the possible association with a suppressed polyol pathway, the current study was designed to investigate the metabolic changes occurring in the renal cortex and to perform a routine assessment of the pathological and functional changes of the kidney in model animals. The *db/db* mice were used as DN animals and were exposed to epalrestat; metabolites in the plasma, renal cortex, and urine were profiled using a gas chromatography–mass spectrometry (GC/MS)-based metabolomic platform. We aimed to elucidate the effect of epalrestat on the metabolic pathway and the relevance to its renal protection effects in *db/db* mice.

MATERIALS AND METHODS

Materials and reagents

Myristic-1,2-¹³C₂ acid, 99 atom% ¹³C, the stable-isotope-labeled internal standard compound, methoxamine hydrochloride (purity 98%), pyridine (≥99.8% GC), formaldehyde solution (36.5–38% in H₂O), and glutaraldehyde solution (grade I, 25% in H₂O) were purchased from Sigma-Aldrich (St. Louis, MO, USA). *N*-methyl-*N*-trimethylsilyl-trifluoroacetamide (MSTFA) plus 1% trimethylchlorosilane (TMCS) were provided by Pierce Chemical (Rockford, IL, USA). Urease was obtained from Sigma. Methanol and *n*-heptane were HPLC grade and obtained from Tedia (Fairfield, OH) and Merck (Darmstadt, Germany), respectively. Purified water was produced by a Milli-Q system (Millipore, Bedford, MA, USA). RIPA

buffer and proteinase inhibitor cocktail were purchased from Sigma-Aldrich. PVDF membrane was purchased from Bio-Rad Laboratories (Hercules, CA, USA). AR (ab175394) antibody, fibronectin (ab2413) antibody, CTGF (ab6992) antibody, TGF-β1 (ab64715) antibody, collagen III (ab7778) antibody, nephrin (ab216341) antibody, podocin (ab50339) antibody, and β-actin antibody (ab8227) were from Abcam (Cambridge, U.K.). Epalrestat (5-[(1Z,2E)-2-methyl-3-phenylpropenylidene]-4-oxo-2-thioxo-3-thiazolidine acetic acid) was provided from Hailing Pharmaceutical Co. Ltd., China.

Animal treatment

Six-week-old male *db/db* mice (BKS.Cg-*Dock7*^{tm+/+}*Lep^{db}*/JNju) and lean wild-type (WT) littermates were purchased from the Model Animal Research Center of Nanjing University. Experimental procedures involving the use of animals complied with the Guidelines for Animal Experimentation of the China Pharmaceutical University, Nanjing, China, and the protocol was approved by the Animal Ethics Committee of that institution. Animals were housed in controlled environmental conditions (temperature, 22 ± 2 °C; humidity, 55% ± 10%), with fixed 12-h light to 12-h dark cycles with free access to water and food.

After adaptation to standard laboratory conditions for 2 weeks, the experimental mice were randomly allocated to the following groups (*n* = 8 per group): WT mice fed regular chow (China Experimental Animal Food Standard, GB 14924.2–2001 and GB 14924.3–2001, Trophic Animal Feed High-tech Co. Ltd., Nantong, China), *db/db* mice fed regular chow, and *db/db* mice fed regular chow supplemented with epalrestat (5-[(1Z,2E)-2-methyl-3-

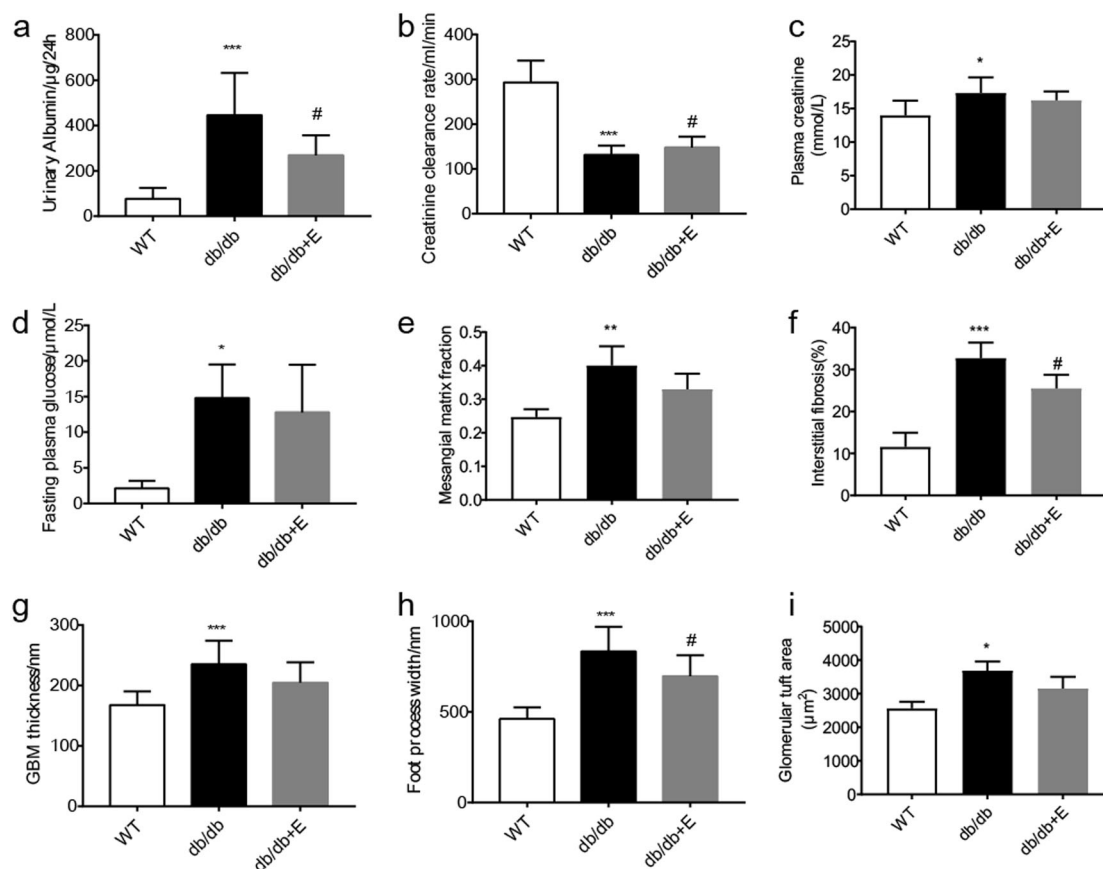


Fig. 1 Biochemical assay of renal function and histological morphology data in different groups of mice. (a) Urinary albumin excretions, (b) creatinine clearance rate, (c) plasma creatinine levels, (d) plasma fasting glucose levels, (e) mesangial matrix fractions, (f) interstitial fibrosis area ratios, (g) glomerular basement membranes thickness, (h) foot process width, (i) glomerular tuft area. The data are expressed as the mean ± SD. **P* < 0.05, ****P* < 0.001 vs. WT group; #*P* < 0.05 vs. *db/db* group

phenylpropenylidene]-4-oxo-2-thioxo-3-thiazolidine acetic acid) at a final concentration of 0.08% (w/w) (*db/db* + epalrestat group). Epalrestat was provided from Hailing Pharmaceutical Co. Ltd., China. All chows were produced by Trophic Animal Feed High-tech Co. Ltd., Nantong, China. The treatment period was 8 weeks.

Sample collection

Each urine sample was collected in a 10-mL tube over an ice bath for 24 h at 16 weeks of age in metabolic cages (Suzhou Fengshi Laboratory Animal Equipment, Suzhou, China), individually. The volume was measured and recorded for each sample. Blood samples were collected after overnight fasting. For each mouse, 0.3 mL blood was collected and added in an anticoagulation tube immediately after the urine collection. After centrifuging at 1000×*g* for 10 min, plasma was prepared and stored at −80 °C until use.

Immediately after blood collection, the mice were sacrificed. The kidneys were dissected and rinsed in cold phosphate buffer solution. The left kidneys were split into two parts in an ice bath. One portion was fixed in 10% formalin for histopathological examination. Sections of the renal cortex (1 × mm³ in volume) were dissected from the other portion and then fixed in 2.5% glutaraldehyde followed by postfixation in 1% osmic acid for assays using electron microscopy. The right kidneys were dissected on an ice plate to separate the cortical and medullar

portions. All non-fixed renal tissues were immediately snap-frozen in liquid nitrogen and stored at −80 °C for later analysis.

Morphology examination

The fixed renal tissues were embedded in paraffin and were then cut into 5-μm-thick sections. Renal sections were deparaffinized in xylene, rehydrated in graded ethanol and then stained with periodic acid-schiff (PAS) and Masson's trichrome following standard protocols. The examination of slides was performed under light microscopy by a pathologist blinded to the experimental profile. PAS were used to assess mesangial expansion (mesangial matrix fraction) in 20 glomeruli (×400) per sample, and tubulointerstitial fibrosis was evaluated by percent of Masson's trichrome positive staining areas in 20 cortical fields (×100) per sample. Briefly, the outline of the glomerular tuft was traced, and the computed area was used as a measure of total glomerular area. The area covered by PAS-positive staining in the same glomerulus was then determined. Mesangial matrix fraction was calculated as the area of positive PAS staining divided by total glomerular tuft area. The percentage of interstitial fibrosis area was calculated from the area occupied by trichrome-stained interstitium divided by the total area [18, 19]. For electron microscopy, samples of the renal cortex were fixed in 3% glutaraldehyde in 0.1 M cacodylate buffer solution (pH 7.4) and fixated in 1% osmium tetroxide phosphate buffer solution. The

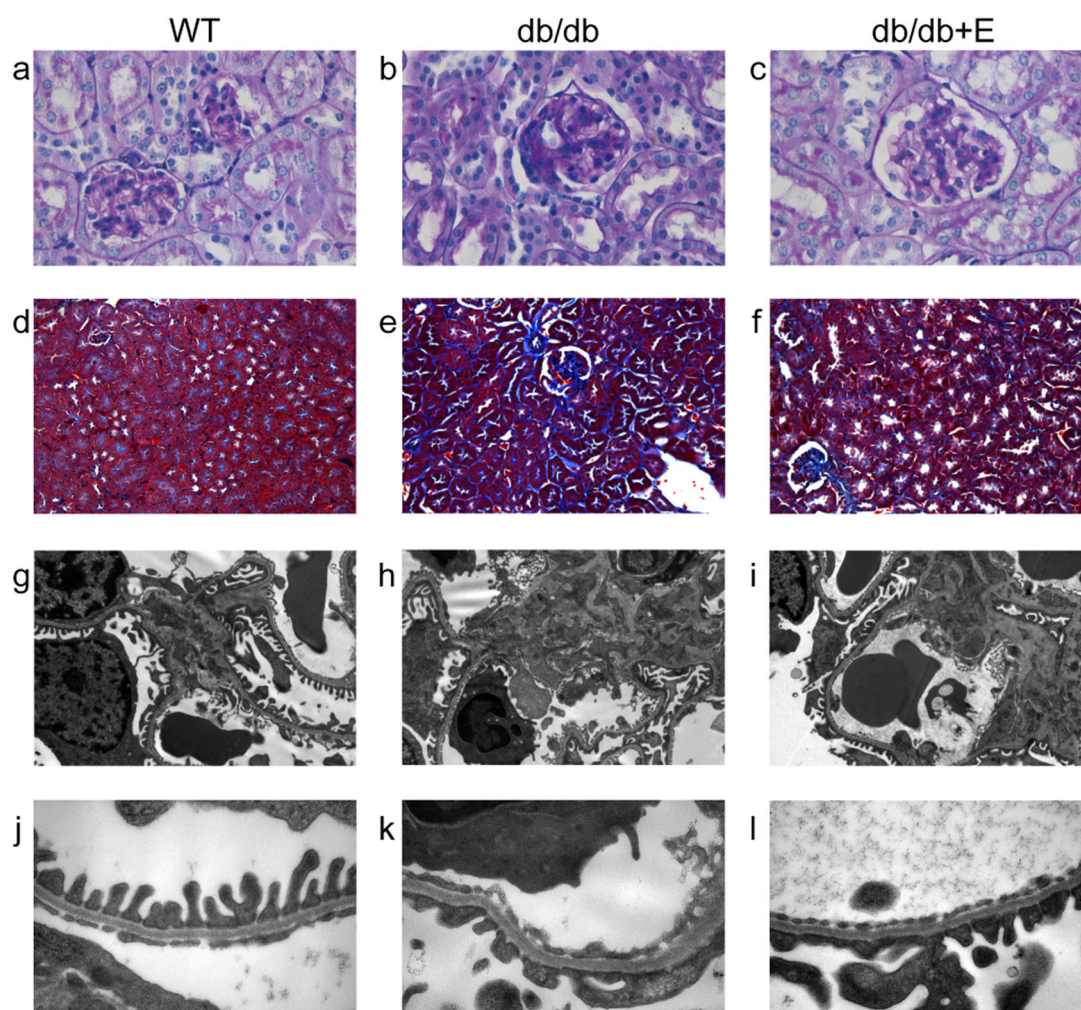


Fig. 2 Histological morphology and ultrastructural inspection of the nephric lesions of mice. **a–c** PAS staining and **d–f** Masson's trichrome staining, ×400 magnification; **g–i** representative TEM images, ×1500 magnification and **j–l** ×7000 magnification

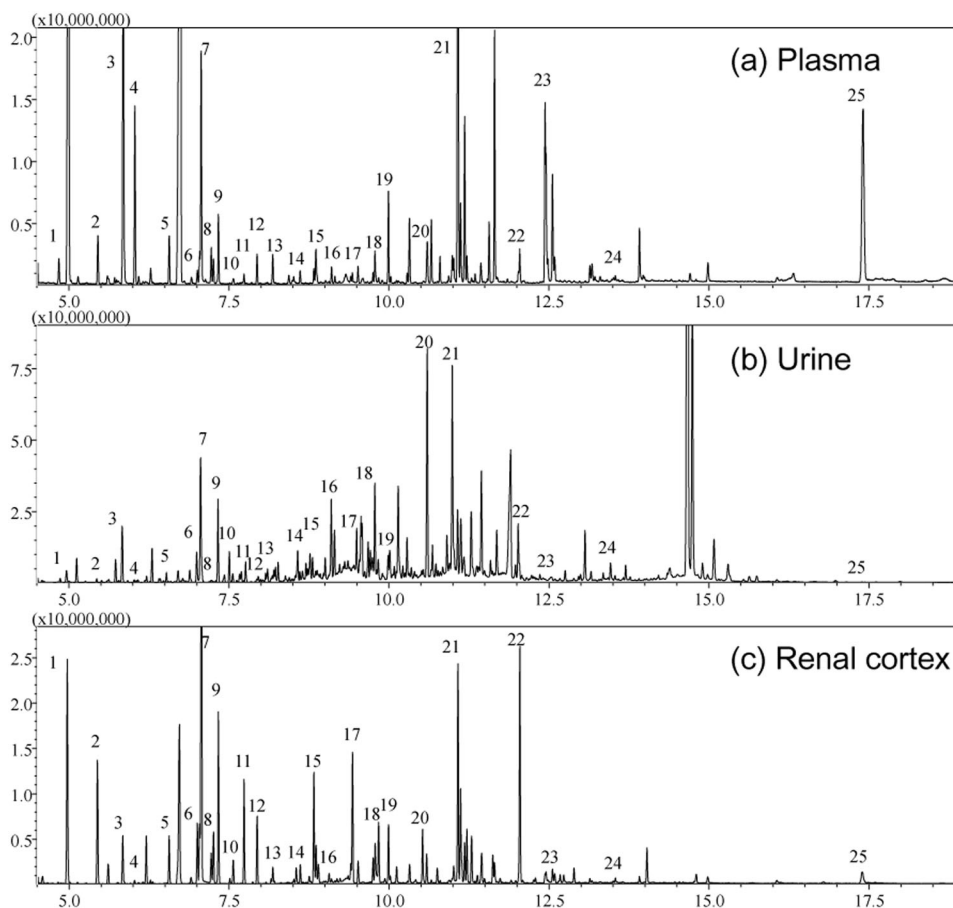


Fig. 3 Typical GC/MS chromatograms of the extracted molecules from the plasma, urine, and renal cortex of the mice. **(a)** Plasma, **(b)** urine, and **(c)** renal cortex. Typical compounds are identified and numbered as follows: 1. Lactate, 2. L-Alanine, 3. Oxalic acid, 4. 3-Hydroxybutyrate, 5. Valine, 6. Leucine, 7. Phosphate, 8. Proline, 9. Glycine, 10. Uracil, 11. Serine, 12. Threonine, 13. 3-Amino-isobutyrate, 14. Malate, 15. Hydroproline, 16. Creatinine, 17. Ornithine, 18. Taurine, 19. Glutamine, 20. Citrate, 21. Glucose, 22. Myo-inositol, 23. Oleic acid, 24. Arachidonic acid, 25. Cholesterol

samples were then dehydrated in a graded series of ethanol and embedded in epoxide resin. Ultrathin sections were stained with uranyl acetate and lead citrate and were examined under a Hitachi 7500 electron microscope (Hitachi, Japan) [20, 21]. Glomerular basement membrane (GBM, 8 photographs in each sample) was measured using the grid intersect method [22], and the average podocyte foot process width (6 photographs in each sample) was measured [23]. From each picture, the GBM was traced and measured, and the number of podocyte foot processes along the GBM was counted by hand. The average podocyte foot process width = $(\pi/4) \times (\Sigma \text{GBM length} / \Sigma \text{number of foot process})$. Then, 1-cm-interval grid line image was overlapped with the capillary loop, and the intersection of grid lines with the endothelial aspect of the glomerular capillary basement membrane determined the point of measurement. Histological analysis was performed in a blinded manner, using ImageJ (Fiji distribution package).

Biochemical analysis

The creatinine clearance rate (Ccr) was estimated by the 24-h urine creatinine and plasma creatinine concentrations, which were measured using a Creatinine Assay Kit (ab65340, Abcam plc., Shanghai, China). Fasting glucose was measured in a similar manner (ab65333, Abcam plc., Shanghai, China), and urine albumin was detected by ELISA (ab108792, Abcam plc., Shanghai, China).

Sample preparation for metabolomic analysis

Frozen renal cortex tissue samples (20 mg) were ground to a homogeneous powder using a liquid nitrogen-chilled mortar and rapidly transferred to a 1.5-mL microcentrifuge tube. Nine-hundred microliters of methanol containing the internal standard, [$^{13}\text{C}_2$]-myristic acid (12.5 $\mu\text{g}/\text{mL}$), was added to each tube. The mixture was vigorously vortexed for 3 min and centrifuged at 20,000 $\times g$ for 10 min at 4 $^\circ\text{C}$. For plasma, 50 μL of samples were added to 200 μL of methanol containing the internal standard and vigorously vortex extracted and centrifuged. For urine samples, 30 μL of urine was first added to 30 μL urease solution (20 U) to decompose the excessive urea in the urine, and then the mixture was added to methanol, vigorously vortex extracted, and centrifuged.

An aliquot of 100 μL of supernatant was transferred to a gas chromatography (GC) vial and evaporated to dryness using a SPD2010-230 SpeedVac Concentrator (Thermo Savant, Holbrook, USA). The dried residue was then dissolved in 30 μL of methoxyamine in pyridine (10 mg/mL) and vigorously vortexed for 2 min. The methoximation reaction was carried out for 16 h at room temperature, followed by trimethylsilylation for 1 h by adding 30 μL of *N*-methyl-*N*-(trimethylsilyl) trifluoroacetamide (MSTFA) with 1% TMCS as the catalyst. Finally, the solution was vortex-mixed again for 30 s after adding the external standard, methyl myristate in heptane (30 $\mu\text{g}/\text{mL}$), to each GC vial for the GC-mass spectrometry (MS) analysis.

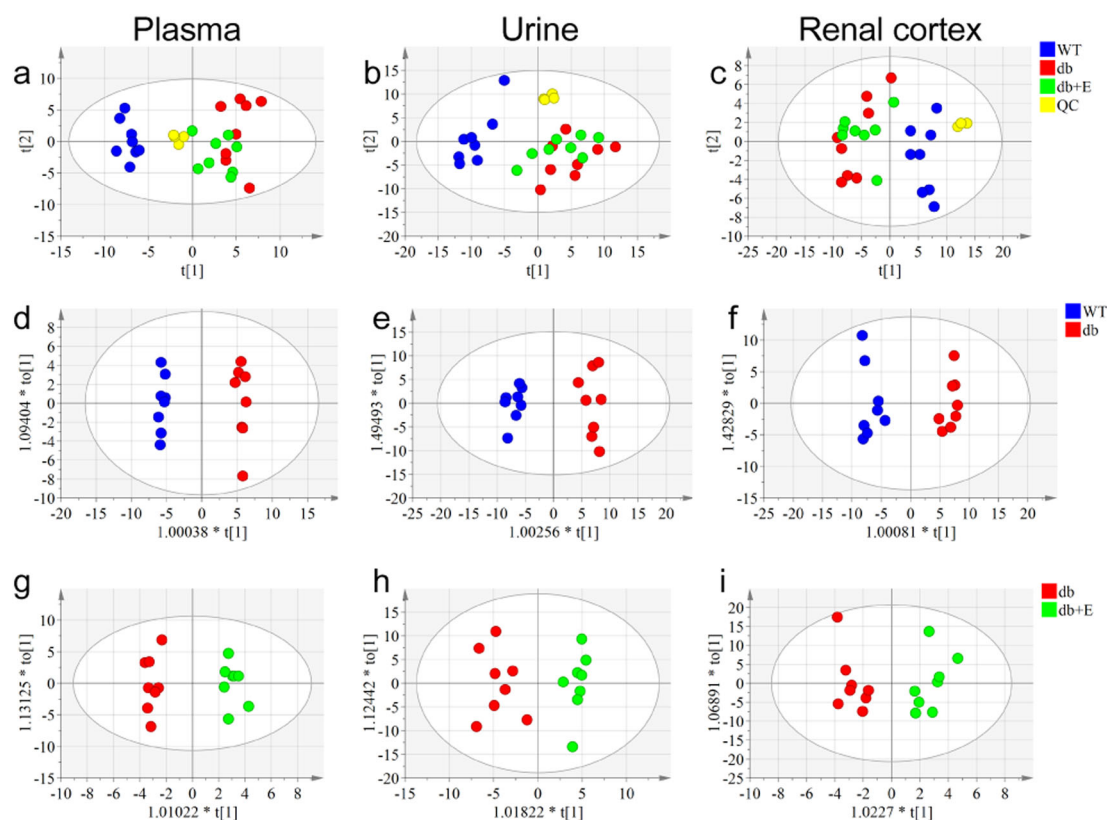


Fig. 4 Metabolic patterns of the three groups of mice based on multivariate statistical analysis of the GC/MS data. Score plots of the three groups and their PCA models for plasma data (a), urine data (b), renal cortex data (c); *db/db* vs. WT groups and their OPLS-DA models for plasma data (d), urine data (e), renal cortex data (f); epalrestat treatment vs. *db/db* groups and their OPLS-DA for plasma data (g), urine data (h), renal cortex data (i)

Table 1. Parameters associated with each model as referred to in Fig. 4

Model number	Type	Components	R2X (cum)	R2Y (cum)	Q2 (cum)
a	PCA-X	3	0.441		0.155
b	PCA-X	4	0.664		0.434
c	PCA-X	3	0.646		0.474
d	OPLS-DA	1 + 1 + 0	0.38	0.995	0.944
e	OPLS-DA	1 + 1 + 0	0.53	0.97	0.937
f	OPLS-DA	1 + 1 + 0	0.643	0.968	0.871
g	OPLS-DA	1 + 1 + 0	0.201	0.974	0.451
h	OPLS-DA	1 + 1 + 0	0.441	0.916	0.595
i	OPLS-DA	1 + 1 + 0	0.53	0.906	0.627

GC/MS analysis

GC/MS analysis was performed, as previously described [24]. In brief, chromatographic separation of the analytes was achieved with a Shimadzu GCMSQP2010 (Shimadzu Corp., Tokyo, Japan) equipped with a RTx-5MS column (30 mm × 0.25 mm i.d. fused-silica capillary column chemically bonded with a 0.25- μ m cross bond, 5% diphenyl/95% dimethyl polysiloxane, Restek Corporation, PA, USA). Helium was used as the carrier gas, and the temperature was initially set at 80 °C for 3 min and then increased to 300 °C at 20 min. Once the temperature reached 300 °C, it was maintained for another 3 min. The eluate was introduced through the transfer line into the mass spectrometer, where the molecules

were ionized with a current beam of 70 eV. The masses were scanned over m/z 50–700 with a detector voltage of –1050 V. To minimize systematic variations, all samples were analyzed in a randomized order, and the quantitative data were normalized to the internal standard. The metabolites were identified by automatically comparing the MS spectra, in-source fragments, and ion features of each peak in the experimental samples with those of reference standards or those available in libraries, such as mainlib and publib in the National Institute of Standards and Technology (NIST) library 2.0(2012), Wiley 9 (Wiley-VCH Verlag GmbH & Co. KGaA, Weinheim, Germany), the in-house mass spectra library database established by Umeå Plant Science Center (Umeå University, Sweden) and our own Laboratory at China Pharmaceutical University.

Metabolomic data processing

The relative quantitative results (peak areas) of all detected peaks were first normalized by the internal standard compound mentioned previously. Urinary data were further weighted by urinary volume [25], and renal cortex data were weighted by the mass of tissues. Multivariate statistical analysis has been widely applied in our former metabolomic studies [26]. Briefly, the resulting matrix, including the compound index as variable names, sample ID as observations, and normalized peak areas (variables), was introduced into the SIMCA Software package (Umetrics, Umeå, Sweden) for multivariate statistical analysis. The data matrix was subjected to conduct by principal component analysis (PCA) to visualize general clustering, trends, or outliers among the observations. In PCA, large numbers of variables (i.e., “high dimensional data”) are reduced to components or eigenvalues that represent combinations of variables that account for most of

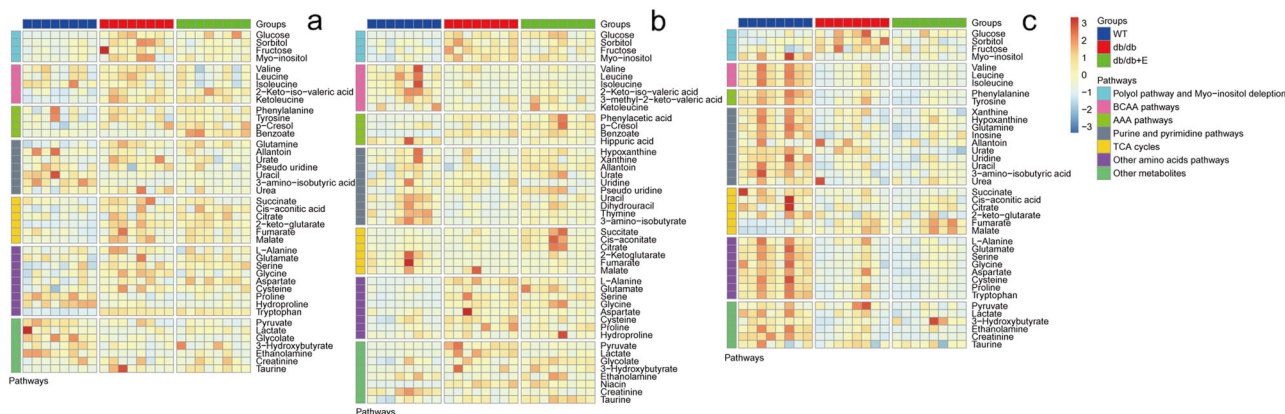


Fig. 5 Heatmap visualizing the intensities of differential metabolites in the plasma (a), urine (b), and renal cortex extracts (c) of mice

the variation in the data. These components also have weightings or “eigenvectors” that indicate the weight of each variable within a component. The different components are intended to be independent of one another (“orthogonal”) so that they capture the unique aspects of the variation in the data. PCA, unlike Factor Analysis, does not assume a formal statistical model, and therefore, assumptions such as multivariate normality are unnecessary [27]. Another way of analyzing multivariate changes is linear discriminant analysis (LDA), which attempts to identify a linear equation that combines the metabolomic variables, with different weightings, in order to predict if the animals belong to a certain group. Partial least squares discriminant analysis (PLS-DA, equivalent to “projection to latent structures DA”) is a method that uses partial least squares regression in the discriminant analysis and can be used to elucidate the separation between groups of variables [28]. In orthogonal projection to latent structures DA (OPLS-DA), an extension of PLS-DA, the data from the continuous variables in the discriminant analysis function are separated into those that are predictive of the dependent variable (e.g., WT or *db/db*) and those that are not, resulting in enhanced diagnostics. OPLS-DA was utilized to validate the PCA model and identify the differential metabolites in urine, plasma or the renal cortex of *db/db* mice vs. WT, and epalrestat treatment *db/db* mice vs. *db/db* mice [29]. The goodness of fit for a model was evaluated using three quantitative parameters as follows; i.e., R2X, the explained variation in X, R2Y, the explained variation in Y, and Q2Y, the predicted variation in Y based on the model using cross-validation [30]. The range of these parameters is between 0 and 1; the closer they approach 1, the better they can be predicted or explained. Variable importance was used to summarize the importance of the X-variables, both for the X- and Y-models and was measured by the variable influence on projection (VIP). The VIP value is a parameter indicating the importance of a variable that contributes to the model. In a model, one can compare the VIP of one variable to the others. Variables with a large VIP, larger than 1, are the most relevant for explaining Y. In addition, the related metabolic pathway based on differential metabolites picked up was searched in Kyoto Encyclopedia of Genes and Genomes (KEGG) (<http://www.genome.jp/kegg/ligand.html>).

Western blot

Randomly selected frozen renal cortex samples from each group of mice were homogenized in RIPA buffer (proteinase inhibitor cocktail added). Approximately 40 µg lysate proteins were separated on a 10% SDS-PAGE gel and then transferred to a PVDF membrane. The membrane’s non-specific binding sites were blocked at room temperature for 1 h with 0.5 g/L non-fat milk powder in Tris-buffered saline/Tween-20 (TBST) and then incubated overnight at 4 °C with primary antibodies. After washing

with TBST, the membranes were incubated with secondary antibodies for 1 h at room temperature with shaking. After washing, the protein bands were detected and analyzed using a ChemiDoc™ MP Imaging System (Bio-Rad Laboratories, CA, USA). β-actin was used as a loading control. The results were expressed as the integrated optical density relative to β-actin. Three repeated experiments were processed for statistics.

Immunohistochemistry

Kidney paraffin sections (4 µm) were mounted on slides, dewaxed, and rehydrated. Slides were brought to the boil in Tris EDTA buffer for 20 min and cooled at room temperature. After 3% hydrogen peroxide treatment for 10 min, the sections were blocked with 1% BSA for 30 min, followed by the incubation of primary antibody for 1 h at 37 °C. The sections were then washed with rinse buffer and incubated with HRP-Polymer Conjugated anti-Mouse/Rabbit IgG complex (Maixin-Bio, Fuzhou, China) for 30 min at room temperature. Localization of peroxidase conjugates was determined using diaminobenzidine tetrahydrochloride solution as chromogen and counterstained with hematoxylin. Ten cortical fields (×100) per sample were analyzed, and results were expressed as average integrated optical density per area (IOD/Area, AOD) value relative to WT groups.

Statistical analysis

Statistical analysis was conducted using SPSS 19.0 (IBM, USA). The data are expressed as the mean ± SD. Statistical differences between the two groups were analyzed using the unpaired Student’s *t*-test. Differences among multiple groups were analyzed using one-way ANOVA.

RESULTS

Biochemical parameters

Compared to the WT group, the *db/db* mice showed an elevated urinary albumin excretion rate (UAER) (Fig. 1a). Glomerular filtration dysfunction was featured by a decreasing Ccr (Fig. 1b, c). There was a significantly elevated fasting plasma glucose level (Fig. 1d) at 16 weeks of age, but no significant change in the plasma glucose level in the epalrestat treatment group compared to the *db/db* group. The UAER value was significantly down-regulated, whereas the decline in Ccr was restrained in the epalrestat treatment group vs. the *db/db* group.

Histopathological and electron micrographic inspection of the microstructure in the renal cortex

Histological sections of kidney tissue stained with PAS and Masson’s trichrome were examined microscopically to evaluate the structural injury in the kidney (Fig. 2a–f). In comparison with

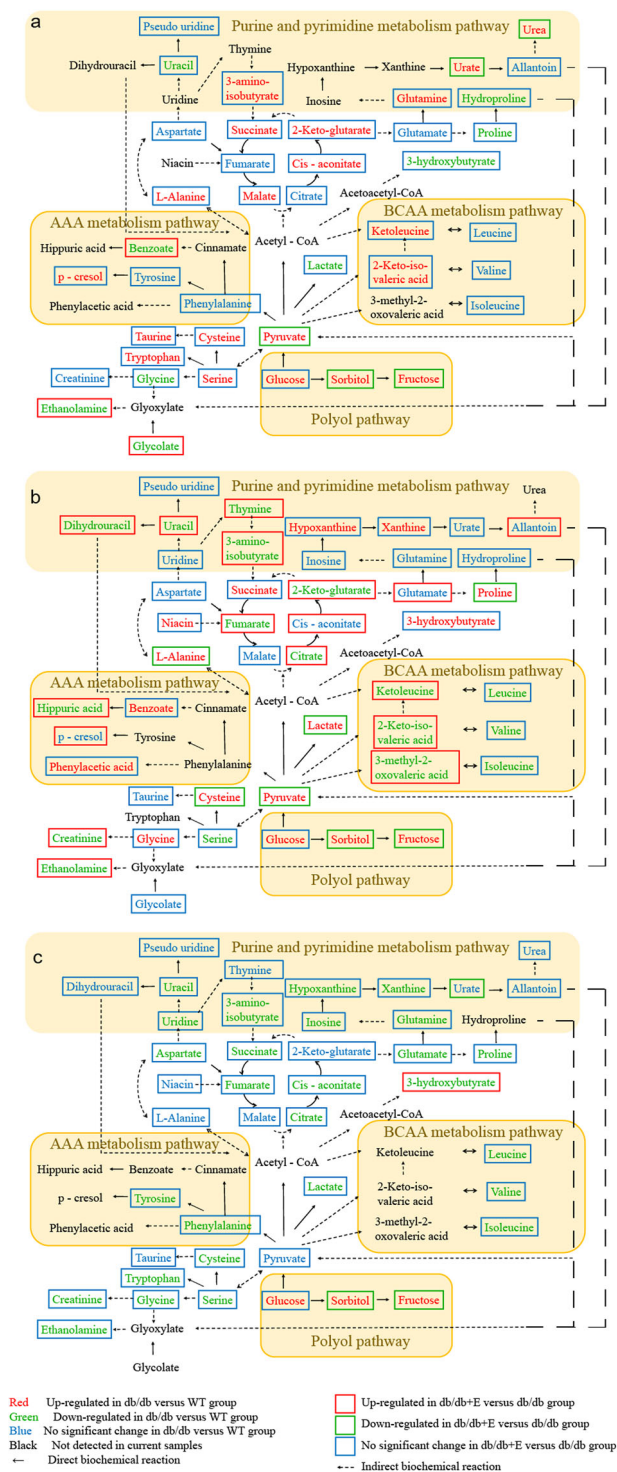


Fig. 6 The differential metabolites and associated metabolic pathways involved in *db/db* mice and the treatment with epalrestat in plasma (a), urine (b), and renal cortex extracts (c) of the mice

the normal controls, elevated mesangial expansion (PAS-positive staining) and an increase in the total glomerular volume were observed in the *db/db* mice (Fig. 1e). Interstitial fibrosis (Masson's trichrome positivity) was widely observed in the *db/db* group (Fig. 1f). By electron microscopy (Fig. 2g–i), the GBMs were observed to be irregularly thickened (Fig. 1g), and diffuse mesangial matrix deposits were seen in the *db/db* mice. Increased

foot process width, indicating foot process fusion, and effacement, was seen when the podocytes were examined (Fig. 1h).

The epalrestat treatment group showed amelioration in GBM thickening and mesangial matrix deposition, though not significantly (Fig. 1e–g). By electron microscopy, we found significant amelioration of podocyte foot process fusion. Meanwhile, interstitial fibrosis areas were rarely spotted in treated mice.

Metabolomic profile of the GC/MS data

The GC/MS analysis of the plasma, urine, and renal cortex extracts revealed a large number of peaks. Deconvolution of the plasma chromatograms produced a total of 130 distinct peaks, and 94 were authentically identified by comparing the mass spectrum of the peak with that available in the libraries and that of the reference compounds. These peaks included amino acids, small organic acids, carbohydrates, fatty acids, lipids, and amines. To acquire the quantitative data, a feature mass (*m/z*) was chosen for each peak, and the peak area was obtained for each deconvoluted peak/molecule. A similar approach was processed for the urine and renal cortex extract chromatograms. There were 154 distinct peaks from the urine samples that were deconvoluted, with 107 identified, and 84 metabolites were identified from 124 peaks from the renal cortex extracts. Typical plasma, urine and renal cortex extract chromatograms from WT mice are shown in Fig. 3. As mentioned in the methods section, to verify the stability of the analysis system, standard deviations of both the internal standard ($[^{13}\text{C}_2]$ myristic acid) and the external standard (methyl myristate) were evaluated. We observed fairly good reproducibility for the two standards in the serum samples (<5%); however, the standard deviations were larger in the urine samples and the renal cortex extracts (<10%) because the urine samples were either diluted or concentrated, depending on the urinary volumes of each mouse and because the weight of the analyzed renal cortex samples varied more. However, the data matrices of the peak areas from the urine and renal cortex were further weighted according to the protocols in the methods section.

Multivariate statistical analysis of the metabolic patterns

The data matrices of the molecules in the samples from the plasma, urine, and renal cortex were initially analyzed using PCA. PCA score plots, in which the scores for PC2 (i.e., *t* [2]) were plotted against those for PC1 (*t* [1]), were used to show the distribution of the analyzed samples containing the information from all the metabolites in the three bio-samples (Fig. 4a–c). According to the PCA algorithm, each dot represents the summarized information from all molecules measured in a single sample. Therefore, the distance between dots indicates the similarity of the metabolic composition between samples, i.e., the closer the dots cluster together, the more similar they will be. Quality control (QC) samples assembled closely, suggesting good repeatability in the GC/MS analysis of the samples. The *db/db* group and WT group were clearly separated in the PCA score plots, which indicated that the group differences were remarkable, and there was a marked deviation of urinary metabolites in the *db/db* group. Moreover, the PCA analysis showed that the epalrestat treatment group moved slightly closer to the WT group, suggesting the treatment effects of epalrestat to some extent. The OPLS-DA analysis was processed as a pattern recognition approach to maximize class separation and recognize the differential metabolites from the WT group vs. the *db/db* group (Fig. 4d–f) and the epalrestat-treated group vs. the *db/db* group (Fig. 4g–i). The OPLS-DA score plots presented good fitness and high predictability of models, indicating that the metabolic profiles changed significantly. In addition, though the R2Y values of all OPLS-DA models were over 0.9, the Q2 values of the WT-*db/db* models (0.8–0.9) were significantly higher than those of the *db/db*-*db/db* + E models (0.4–0.6), suggesting that the metabolic shift resulting from epalrestat treatment was obvious

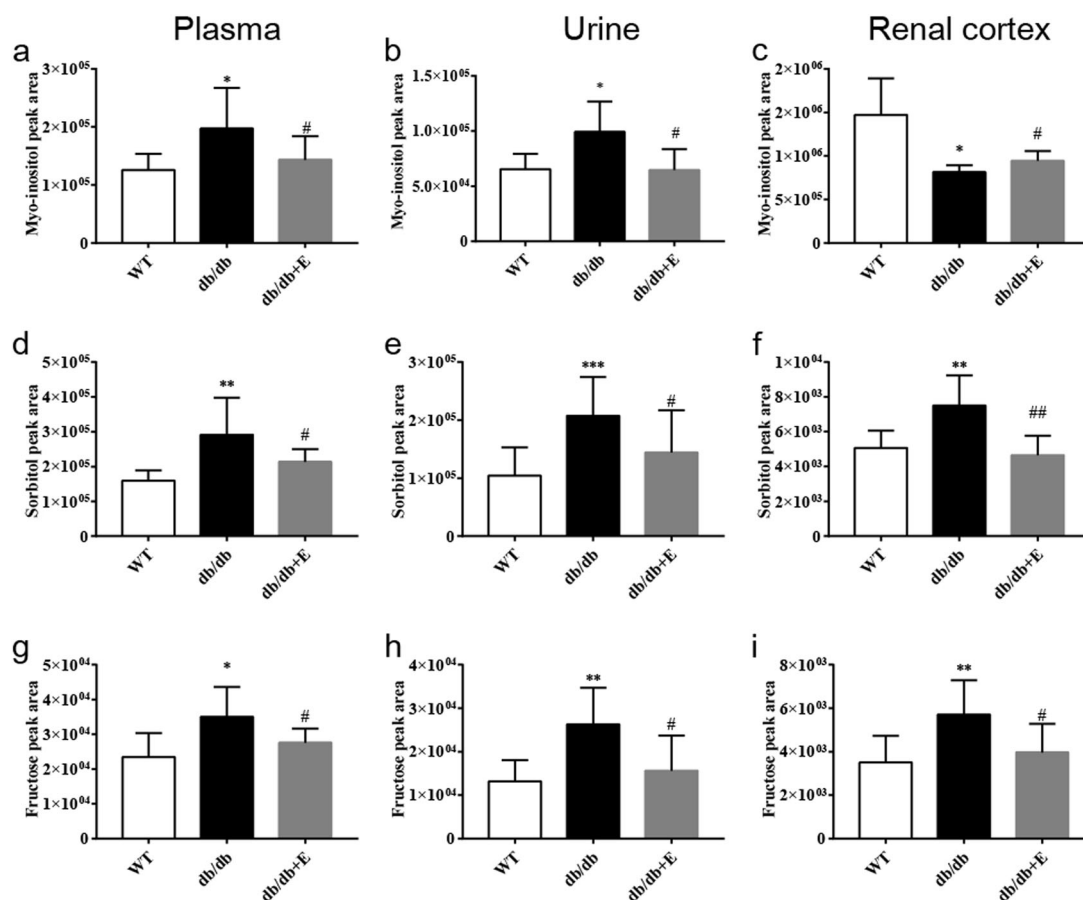


Fig. 7 Relative abundance of myo-inositol, sorbitol, and fructose in the plasma, urine, and renal cortex of the mice. Myo-inositol (a–c), sorbitol (d–f), and fructose (g–i) levels change in plasma, urine, and renal cortex extracts measured directly by GC/MS peak areas. The data are expressed as the mean ± SD. * $P < 0.05$, ** $P < 0.01$, *** $P < 0.001$ vs. WT group; # $P < 0.05$, ## $P < 0.01$ vs. *db/db* group

(Table 1) and partly regulated by the epalrestat effect on the perturbed metabolic pattern of the *db/db* mice.

Perturbed metabolites in urine and the renal cortex involved in polyol pathway

The perturbed metabolites in the plasma, urine, and renal cortex were screened and selected for both *db/db* mice (*db/db* vs. WT) and the treatment with epalrestat in *db/db* mice (*db/db*+E vs. *db/db*). Variable importance in the projection (VIP) of the OPLS-DA model was generated using Pareto scaling [31] to identify the metabolite contribution to the discrimination. The metabolites with a VIP value above 1.0 and a *p*-value below 0.05 were considered differentially perturbed metabolites. Heatmaps were generated for each sample species to visualize the intensities of differential metabolites in different groups (Fig. 5). Based on pathway analysis in the KEGG database, the differential metabolites suggested the perturbed metabolic pathways, including the TCA cycle, amino acid metabolism, purine and pyrimidine metabolism, and others (Fig. 6).

Polyol pathway metabolites and myo-inositol levels were significantly changed in the plasma, urine, and renal cortex for both the *db/db* mice and those after treatment with epalrestat (Fig. 7). In detail, we confirmed that the sorbitol and fructose were elevated in the plasma, urine, and renal cortex of *db/db* mice, and all their levels were downregulated after intervention with epalrestat (Fig. 7d–i). It was indicated that *db/db* mice increased production of the two metabolites in vivo, and there were elevated osmolytes in the renal cells of the *db/db* mice. After treatment with epalrestat, the production of the two metabolites

was depressed, and the osmotic stress in renal cells was alleviated. Simultaneously, there was significantly elevated myo-inositol in the biofluids, i.e., plasma and urine, of the *db/db* mice (Fig. 7a, b), although the myo-inositol level in the renal cortex greatly decreased (Fig. 7c). Treatment with epalrestat reduced myo-inositol in the plasma and urine, whereas the myo-inositol level increased in the renal cortex (Fig. 7a–c). AR downregulation in the renal cortex was checked by Western blot (Fig. 8a, b). Fibronectin (Fig. 8c), TGF-β1 (Fig. 8d), collagen III (Fig. 9b), and CTGF (Fig. 9e) were overexpressed. Podocyte injury was also indicated by underexpression of nephrin and podocin (Fig. 8e, f).

DISCUSSION

Osmotic metabolites involved in the polyol pathway in *db/db* mice

Cellular glucose is primarily metabolized through the glycolysis pathway and then the Krebs cycle to produce the energy for cells that is normally required. Under hyperglycemic conditions, however, the increased amount of glucose activates AR and the polyol pathway to produce an excessive amount of sorbitol [32–34]. Because intracellular sorbitol is difficult to diffuse across cell membranes, the accumulated intracellular glucose and sorbitol, together with the downstream metabolite fructose, promote osmotic stress in cells, which is considered the pathogenic mechanism and responsible for the eventual cellular damage [35, 36]. Excessive amounts of intracellular sorbitol and fructose also induce the depletion of myo-inositol, a crucially important osmotic balance substance. Studies on rat glomerular mesangial

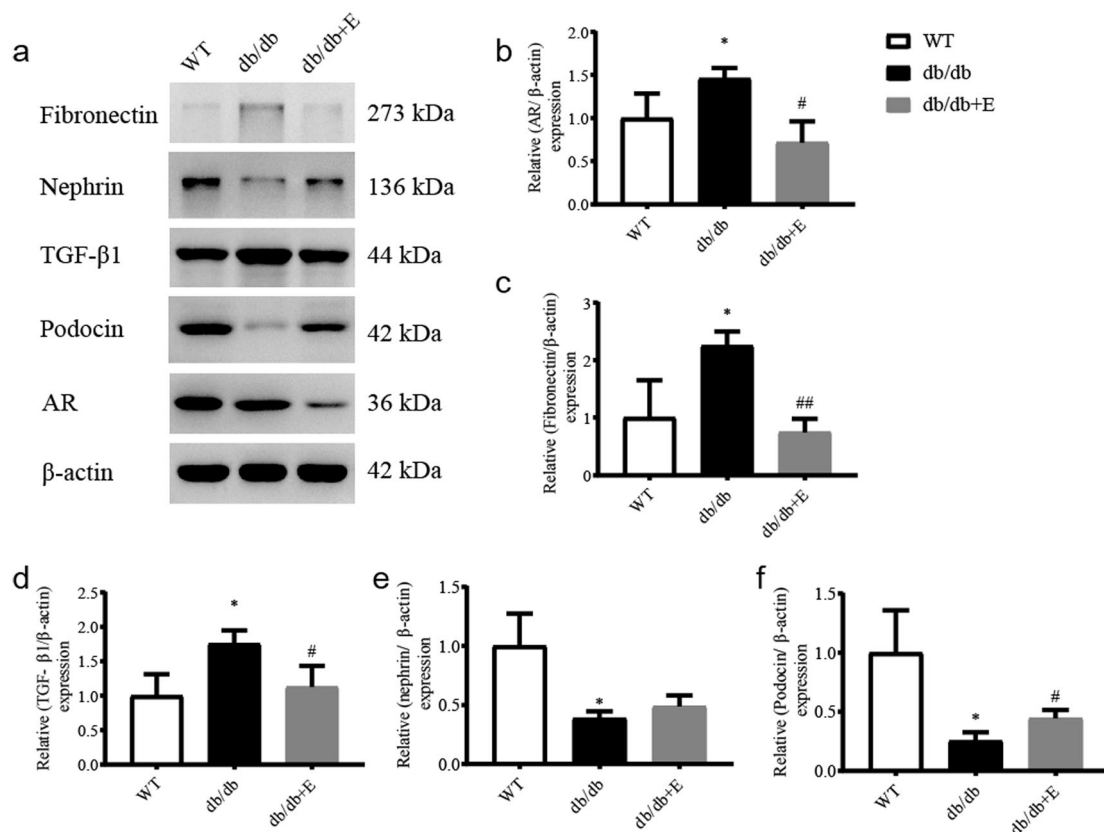


Fig. 8 Western blot analysis (a) of aldose reductase (b), fibronectin (c), TGF-β1 (d), nephrin (e), and podocin (f). The data are expressed as the mean ± SD. **P* < 0.05 vs. WT group; #*P* < 0.05, ##*P* < 0.01 vs. *db/db* group

cells and bovine lens epithelial cells suggested that the uptake of myo-inositol was dependent on and sensitive to intracellular sorbitol, which suggested an elevated sorbitol level in DN-suppressed myo-inositol uptake [37, 38].

In this study, significantly elevated levels of sorbitol and fructose were observed in the plasma, urine, and renal cortex of *db/db* mice. Theoretically, the accumulation of osmolytes inevitably results in the depletion of myo-inositol [7, 8] to maintain cell homeostasis. Consistently, we observed a marked decrease in myo-inositol in the renal cortex and a distinct elevation in myo-inositol in the plasma and urine of the *db/db* mice. These results strongly suggested that there was an extensive activation of AR and the polyol pathway in the *db/db* mice. Additionally, a substantial amount of sorbitol and fructose was produced as a consequence, and a certain amount of myo-inositol intake was suppressed in multiple organs/tissues, including the renal cortex. Studies showed that the depletion of myo-inositol in turn reduced sodium-potassium adenosine triphosphate activity and altered the cellular metabolism and membrane structure of the cells [39], which were observed in the renal cortex of STZ-diabetic rats [15, 16]. It was suggested that the depletion of myo-inositol in the renal cortex contributed to the nephric pathology and dysfunction [40].

Epalrestat showed efficient inhibition of the production of sorbitol, fructose, and homeostasis of intracellular myo-inositol. The myo-inositol level in the plasma and urine markedly decreased in parallel to the levels of sorbitol and fructose, and an increased myo-inositol level was detected in the renal cortex. Together with the observations of the reductions in sorbitol and fructose in the plasma and urine and the increase in myo-inositol in the renal cortex and its decrease in urine, it is strongly suggested that epalrestat reversed the depletion of myo-inositol

at the system level and in the renal cortex tissue of *db/db* mice. It was indicated that the inhibition of the polyol pathway by epalrestat was involved in the renal protective effect of epalrestat on DN.

Renal protective effect of epalrestat and relevance to the inhibition of the polyol pathway
The polyol pathway has long been considered one of the important initiating factors for functional and structural changes in the diabetic kidney [8, 41–43], where AR is the rate-determining enzyme of the two-step polyol pathway [1]. It has been reported that AR could be weakly detected by immunohistochemistry in the renal cortex from non-diabetic individuals, but much stronger glomerular expression could be observed in samples from patients with DN [44–46]. Carolyn et al. assumed that AR played an important role in enhancing renal medullary cells to adapt to osmotic stress [47], although overexpression of AR in the diabetic kidney under hyperglycemia and the production of excess intracellular osmolytes, such as sorbitol, to counterbalance extracellular hypertonicity was a likely physiological or pathological response of AR in DN [48]. In addition, sorbitol can be converted to fructose, which is then metabolized largely by fructokinase, also known as ketohexokinase, leading to ATP depletion, proinflammatory cytokine expression, and oxidative stress. The fructose produced by the polyol pathway can become phosphorylated to fructose-3-phosphate, which is broken down to 3-deoxyglucosone; both compounds are powerful glycosylating agents that enter in the formation of AGE products [49, 50]. Excessive fructose has been suggested as a potential nephrotoxin. Fructose-fed rats develop modest tubulointerstitial injury, and the acceleration of chronic kidney disease (CKD) [51], and fructose supplementation

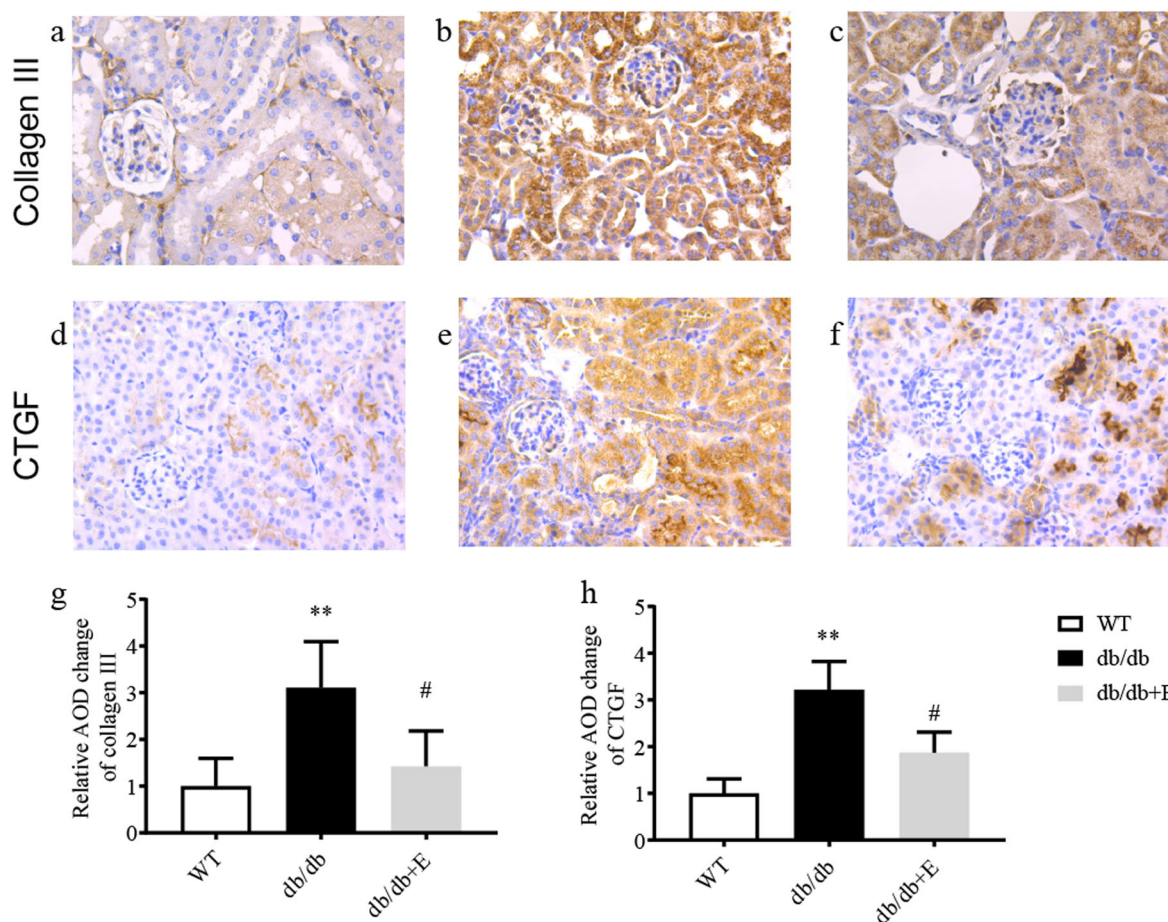


Fig. 9 Representative immunohistochemical staining for collagen III (a–c) and CTGF (d–f) in renal cortex, $\times 100$ magnification, and quantitative analysis of relative AOD, (g) collagen III, and (h) CTGF. The data are expressed as the mean \pm SD. ** $P < 0.01$ vs. WT group; # $P < 0.05$ vs. *db/db* group

accelerates renal disease in the remnant kidney model [52, 53]. In this study, markedly elevated fructose was determined in the plasma, urine, and renal cortex of *db/db* mice, suggesting the activated oxidative stress, and enhanced renal injury. Epalrestat efficiently reduced the level of fructose in the plasma, urine, and renal cortex, which is one of the underlying mechanisms contributing to the effectiveness of epalrestat on DN.

ARs have been investigated for approximately 40 years, with most studies involving endpoints in diabetic neuropathy and retinopathy [54]. In 2011, Yasuhiro et al. [49], found that transgenic mice overexpressing human AR were became diabetic with streptozotocin and showed augmented expression of TonEBP in renocortical tubular cells with vacuolated degenerative changes, and ARI ONO 2235 treatment was partially effective. In 2014, Jie et al. found that AR regulates miR-200a-3p/141-3p to coordinate Keap1-Nrf2, Tgf- β 1/2, and Zeb1/2 signaling in renal mesangial cells and the renal cortex of diabetic mice, which contributed to aberrant regulation in oxidative stress, fibrogenesis, and the epithelial–mesenchymal transition (EMT) [55]. Finally, an ARI, zopolrestat, has been confirmed to be effective in DN by previous research. Although clinical studies of epalrestat on DN were carried out and the effect remained controversial [56], epalrestat significantly reduced albuminuria and ameliorated the podocyte foot process fusion and interstitial fibrosis in the kidneys of *db/db* mice. We hypothesize that the modulation of sorbitol accumulation and myo-inositol depletion through the polyol pathway favors the amelioration of the oxidative stress of the renal cells of

DN. DN patients have great potential to benefit from the agents of ARIs.

Changes in aromatic amino acids, branched amino acids, and purine and pyrimidine metabolism pathways

The levels of 3 branched-chain amino acids (BCAAs, i.e., leucine, isoleucine, and valine) were significantly downregulated in the urine and cortex of *db/db* mice. The levels of branched-chain keto acids (BCKAs), synthetic precursors, keto-leucine, 3-methyl-2-keto-valeric acid, and 2-keto-iso-valeric acid were also lower in the *db/db* mouse urine. Similar phenomena were found in renal interstitial fibrosis rats [57]. BCAAs play large roles in nutritional regulation and are associated with the development of type 2 diabetes, insulin resistance, and chronic kidney disease [58, 59]. The abnormalities of BCAA and BCKA metabolism might be responsible for disturbances in renal amino acid exchanges and subsequent renal dysfunction [60]. Recently, Mi et al. [61], suggested that BCAAs counter oxidative stress in the kidneys of diabetic rats and alleviate diabetic kidney injury via the JNK/TGF- β /MMP-9 pathway, which indicated that a deficiency in branched chain amino acids in the renal cortex could aggravate renal dysfunction due to oxidative stress in DN.

The metabolism of aromatic amino acids, especially phenylalanine and tyrosine, was considered to be correlated with CKD and DN [62, 63]. Changes in phenylalanine metabolism showed a close association with chronic kidney failure, including extensive urinary excretion of its down products [64]. P-Cresol and hippuric acid are end products of the conversion of phenylalanine and tyrosine.

They are protein-bound uremic toxins that contribute to the progression of chronic kidney disease and were shown to induce endothelial reactive oxygen species (ROS) production in human umbilical vein endothelial cells [65]. These urine levels were lower in the *db/db* groups, indicating glomerular dysfunction. Moreover, their excretion disturbance would reasonably aggravate renal function failure.

Compared to the *db/db* mice, in the epalrestat treatment group, urine BCKAs, p-Cresol, and hippuric acid excretion were significantly upregulated, which indicated that glomerular dysfunction was ameliorated. This finding is consistent with the biochemical and histological examinations.

Deficiencies in purines and pyrimidines in the renal cortex and urine were observed. Uridine is a nucleoside present in the pyrimidine metabolism pathway. It is considered a predictor of kidney deterioration. Uridine and its nucleotide, uracil, were observed to effectively suppress renin secretion in the kidney, leading to its vasoconstrictor effect [66]. The lowered excretion of xanthine and hypoxanthine might be due to glomerular dysfunction. However, their levels were not elevated in the renal cortex or plasma, and plasma urate accumulated instead. Apparently, xanthine oxidase oxidatively catalyzed hypoxanthine to xanthine and then to uric acid. This process increased the level of intracellular ROS, which caused renal injury by direct oxidative damage to renal cells and indirectly inducing inflammatory responses by activating the NF- κ B signaling pathway [67]. The excretion levels of these compounds were elevated in the epalrestat treatment group, and we attribute this increase to improved glomerular function. Although the levels of hypoxanthine and xanthine in plasma were not measured by our GC/MS methods, the urate level was significantly controlled in the epalrestat treatment group, indicating that the oxidative stress induced by xanthine oxidase might be reduced.

CONCLUSION

Epalrestat significantly reduced albuminuria, reversed the podocyte fusion process and interstitial fibrosis in the renal cortex of *db/db* mice, inhibited AR, and efficiently reversed the accumulation of the osmolytes in nephritic tissue. It was suggested that epalrestat possesses a renal protective effect on DN and that modulation of the polyol pathway is a potential strategy for the clinical management of DN.

ACKNOWLEDGEMENTS

We want to thank Dr. Xiao-dong Zhu for his help in technical support for transmission electron microscopy study in the Research Institute of Nephrology of PLA, Jinling Hospital, Nanjing, China. This study was financially supported by the National Natural Science Foundation of the People's Republic of China (81530098), the National Key Special Project of Science and Technology for Innovation Drugs of China (2017ZX09301013, 2015ZX09501001), the Natural Science Foundation of Jiangsu Province (BL2014070), and the project of university collaborative innovation center of Jiangsu province (Modern Chinese Medicine Center and Biological Medicine Center).

AUTHOR CONTRIBUTIONS

JH, H-xG, NY, X-dZ, C-hZ, and J-kW performed the experiments; JH and R-bS analyzed the data; JH and J-yA interpreted the results of the experiment, prepared figures, and drafted the manuscript; YX, J-wZ, and FD helped to design the research; J-yA and G-jW revised the manuscript; G-jW approved the final version of the manuscript.

ADDITIONAL INFORMATION

Competing interests: The authors declare that the research was conducted in the absence of any commercial or financial relationships that could be construed as a potential conflict of interest.

REFERENCES

- Oates PJ. Aldose reductase inhibitors and diabetic kidney disease. *Curr Opin Investig Drugs*. 2010;11:402–17.
- Nishikawa T, Edelstein D, Brownlee M. The missing link: a single unifying mechanism for diabetic complications. *Kidney Int Suppl*. 2000;77:S26–30.
- Hers HG. Le mécanisme de la transformation de glucose en fructose par les vésicules séminales. *Biochim Biophys Acta*. 1956;22:202–3.
- Dunlop M. Aldose reductase and the role of the polyol pathway in diabetic nephropathy. *Kidney Int Suppl*. 2000;77:S3–12.
- Yabe-Nishimura C. Aldose reductase in glucose toxicity: a potential target for the prevention of diabetic complications. *Pharmacol Rev*. 1998;50:21–34.
- Van Heyningen R. Formation of polyols by the lens of the rat with 'sugar' cataract. *Nature*. 1959;184:194–5.
- Greene DA, Chakrabarti S, Lattimer SA, Sima AA. Role of sorbitol accumulation and myo-inositol depletion in paranodal swelling of large myelinated nerve fibers in the insulin-deficient spontaneously diabetic bio-breeding rat. Reversal by insulin replacement, an aldose reductase inhibitor, and myo-inositol. *J Clin Invest*. 1987;79:1479–85.
- Greene DA, Lattimer SA, Sima AA. Sorbitol, phosphoinositides, and sodium-potassium-ATPase in the pathogenesis of diabetic complications. *N Engl J Med*. 1987;316:599–606.
- Tang W, Martin K, Hwa J. Aldose reductase, oxidative stress, and diabetic mellitus. *Front Pharmacol*. 2012;3:87.
- Huang Z, Hong Q, Zhang X, Xiao W, Wang L, Cui S, et al. Aldose reductase mediates endothelial cell dysfunction induced by high uric acid concentrations. *Cell Commun Signal*. 2017;15:3.
- Ramirez MA, Borja NL. Epalrestat: an aldose reductase inhibitor for the treatment of diabetic neuropathy. *Pharmacotherapy*. 2008;28:646–55.
- Tsugawa T, Shinohara R, Nagasaka A, Nakano I, Takeda F, Nagata M, et al. Alteration of urinary sorbitol excretion in WBN-kob diabetic rats - treatment with an aldose reductase inhibitor. *J Endocrinol*. 2004;181:429–35.
- Itagaki I, Shimizu K, Kamanaka Y, Ebata K, Kikkawa R, Haneda M, et al. The effect of an aldose reductase inhibitor (Epalrestat) on diabetic nephropathy in rats. *Diabetes Res Clin Pract*. 1994;25:147–54.
- Li M, Wang X, Aa J, Qin W, Zha W, Ge Y, et al. GC/TOFMS analysis of metabolites in serum and urine reveals metabolic perturbation of TCA cycle in *db/db* mice involved in diabetic nephropathy. *Am J Physiol Ren Physiol*. 2013;304:F1317–24.
- Chang HH, Chao HN, Walker CS, Choong SY, Phillips A, Loomes KM. Renal depletion of myo-inositol is associated with its increased degradation in animal models of metabolic disease. *Am J Physiol Ren Physiol*. 2015;309:F755–63.
- Fonteles MC. Myo-inositol concentration is strongly reduced in the renal cortex of STZ-diabetic rats. *FASEB J*. 2017;31:673–4.
- Hotta N, Kawamori R, Fukuda M, Shigeta Y. The Aldose Reductase Inhibitor–Diabetes Complications Trial Study G. Long-term clinical effects of epalrestat, an aldose reductase inhibitor, on progression of diabetic neuropathy and other microvascular complications: multivariate epidemiological analysis based on patient background factors and severity of diabetic neuropathy. *Diabet Med*. 2012;29:1529–33.
- Melhem MF, Craven PA, Liachenko J, DeRubertis FR. α -Lipoic acid attenuates hyperglycemia and prevents glomerular mesangial matrix expansion in diabetes. *J Am Soc Nephrol*. 2002;13:108–16.
- Cao Q, Wang Y, Zheng D, Sun Y, Wang Y, Lee VW, et al. IL-10/TGF- β -modified macrophages induce regulatory T cells and protect against adriamycin nephrosis. *J Am Soc Nephrol*. 2010;21:933–42.
- Pei F, Li BY, Zhang Z, Yu F, Li XL, Lu WD, et al. Beneficial effects of phlorizin on diabetic nephropathy in diabetic *db/db* mice. *J Diabetes Complications*. 2014;28:596–603.
- Liu J, Chen Z, Zhang Y, Zhang M, Zhu X, Fan Y, et al. Rhein protects pancreatic β -cells from dynamin-related protein-1-mediated mitochondrial fission and cell apoptosis under hyperglycemia. *Diabetes*. 2013;62:3927–35.
- Mac-Moune Lai F, Szeto CC, Choi PC, Ho KK, Tang NL, Chow KM, et al. Isolate diffuse thickening of glomerular capillary basement membrane: a renal lesion in prediabetes? *Mod Pathol*. 2004;17:1506–12.
- van den berg JG, van den Bergh Weerman MA, Assmann KJM, Weening JJ, Florquin S. Podocyte foot process effacement is not correlated with the level of proteinuria in human glomerulopathies. *Kidney Int*. 2004;66:1901–6.
- Guo J, Yong Y, Aa J, Cao B, Sun R, Yu X, et al. Compound danshen dripping pills modulate the perturbed energy metabolism in a rat model of acute myocardial ischemia. *Sci Rep*. 2016;6:37919.
- Warrack BM, Hnatyshyn S, Ott KH, Reilly MD, Sanders M, Zhang H, et al. Normalization strategies for metabolomic analysis of urine samples. *J Chromatogr B Biomed Appl*. 2009;877:547–52.
- He J, Zhu Y, Aa J, Smith PF, De Ridder D, Wang G, et al. Brain metabolic changes in rats following acoustic trauma. *Front Neurosci*. 2017;11:148.

27. Manly BfJ, Alberto JAN. *Multivariate statistical methods. A primer.* 4th edn. (Chapman & Hall/CRC, New York, United States, 2016).
28. Tang L, Peng S, Bi Y, Shan P, Hu X. A new method combining LDA and PLS for dimension reduction. *PLoS ONE.* 2014;9:e96944.
29. Wiklund S, Johansson E, Sjöström L, Mellerowicz EJ, Edlund U, Shockey JP, et al. Visualization of GC/TOF-MS-based metabolomics data for identification of biochemically interesting compounds using OPLS class models. *Anal Chem.* 2008;80:115–22.
30. Sedghipour MR, Sadeghi-Bazargani H. Applicability of supervised discriminant analysis models to analyze astigmatism clinical trial data. *Clin Ophthalmol.* 2012;6:1499–506.
31. Worley B, Powers R. Multivariate analysis in metabolomics. *Curr Metab.* 2013;1:92–107.
32. Sango K, Suzuki T, Yanagisawa H, Takaku S, Hirooka H, Tamura M, et al. High glucose-induced activation of the polyol pathway and changes of gene expression profiles in immortalized adult mouse Schwann cells IMS32. *J Neurochem.* 2006;98:446–58.
33. Suzuki T, Mizuno K, Yashima S, Watanabe K, Taniko K, Yabe-Nishimura C, et al. Characterization of polyol pathway in schwann cells isolated from adult rat sciatic nerves. *J Neurosci Res.* 1999;57:495–503.
34. Ferraz M, Ishii-Iwamoto EL, Batista MR, Brunaldi K, Bazotte RB. Sorbitol accumulation in rats kept on diabetic condition for short and prolonged periods. *Acta Pharmacol Sin.* 1997;18:309–11.
35. Kinoshita JH. Cataracts in galactosemia. The Jonas S. Friedenwald Memorial Lecture. *Invest Ophthalmol.* 1965;4:786–99.
36. Kinoshita JH. Mechanisms initiating cataract formation. Proctor Lecture. *Invest Ophthalmol.* 1974;13:713–24.
37. Cammarata PR, Chen HQ, Yang J, Yorio T. Modulation of myo-[3H]inositol uptake by glucose and sorbitol in cultured bovine lens epithelial cells. II. Characterization of high- and low-affinity myo-inositol transport sites. *Invest Ophthalmol Vis Sci.* 1992;33:3572–80.
38. Haneda M, Kikkawa R, Arimura T, Ebata K, Togawa M, Maeda S, et al. Glucose inhibits myo-inositol uptake and reduces myo-inositol content in cultured rat glomerular mesangial cells. *Metabolism.* 1990;39:40–45.
39. Raccach D, Coste T, Cameron NE, Dufayet D, Vague P, Hohman TC, et al. Effect of the aldose reductase inhibitor tolrestat on nerve conduction velocity, NA/K ATPase activity, and polyols in red blood cells, sciatic nerve, kidney cortex, and kidney medulla of diabetic rats. *J Diabetes Complications.* 1998;12:154–62.
40. Croze ML, Soulage CO. Potential role and therapeutic interests of myo-inositol in metabolic diseases. *Biochimie.* 2013;95:1811–27.
41. Kinoshita JH, Nishimura C. The involvement of aldose reductase in diabetic complications. *Diabetes Metab Rev.* 1988;4:323–37.
42. Larkins RG, Dunlop ME. The link between hyperglycaemia and diabetic nephropathy. *Diabetologia.* 1992;35:499–504.
43. Yin XX, Zhang YD, Shen JP, Wu HW, Zhu X, Li LM, et al. Protective effects of bendazac lysine on early experimental diabetic nephropathy in rats. *Acta Pharmacol Sin.* 2005;26:721–8.
44. Kasajima H, Yamagishi SI, Sugai S, Yagihashi N, Yagihashi S. Enhanced in situ expression of aldose reductase in peripheral nerve and renal glomeruli in diabetic patients. *J Peripher Nerv Syst.* 2002;7:134.
45. Corder CN, Braughler JM, Culp PA. Quantitative histochemistry of the sorbitol pathway in glomeruli and small arteries of human diabetic kidney. *Folia Histochem Cytochem (Krakow).* 1979;17:137–45.
46. Sands JM, Terada Y, Bernard LM, Knepper MA. Aldose reductase activities in microdissected rat renal tubule segments. *Am J Physiol.* 1989;256:F563–69.
47. Bondy CA, Lightman SL, Lightman SL. Developmental and physiological regulation of aldose reductase mRNA expression in renal medulla. *Mol Endocrinol.* 1989;3:1409–16.
48. Lorenzi M. The polyol pathway as a mechanism for diabetic retinopathy: attractive, elusive, and resilient. *Exp Diabetes Res.* 2007;2007:61038.
49. Hashimoto Y, Yamagishi S, Mizukami H, Yabe-Nishimura C, Lim SW, Kwon HM, et al. Polyol pathway and diabetic nephropathy revisited: Early tubular cell changes and glomerulopathy in diabetic mice overexpressing human aldose reductase. *J Diabetes Investig.* 2011;2:111–22.
50. Tarr JM, Kaul K, Chopra M, Kohner EM, Chibber R. Pathophysiology of diabetic retinopathy. *ISRN Ophthalmol.* 2013;2013:343560.
51. Nakayama T, Kosugi T, Gersch M, Connor T, Sanchez-Lozada LG, Lanaspas MA, et al. Dietary fructose causes tubulointerstitial injury in the normal rat kidney. *Am J Physiol Ren Physiol.* 2010;298:F712–20.
52. Lanaspas MA, Ishimoto T, Cicerchi C, Tamura Y, Roncal-Jimenez CA, Chen W, et al. Endogenous fructose production and fructokinase activation mediate renal injury in diabetic nephropathy. *J Am Soc Nephrol.* 2014;25:2526–38.
53. Gersch MS, Mu W, Cirillo P, Reungjui S, Zhang L, Roncal C, et al. Fructose, but not dextrose, accelerates the progression of chronic kidney disease. *Am J Physiol Ren Physiol.* 2007;293:F1256–61.
54. Chalk C, Benstead TJ, Moore F. Aldose reductase inhibitors for the treatment of diabetic polyneuropathy. *Cochrane Database Syst Rev* 2007;1:CD004572.
55. Wei J, Zhang Y, Luo Y, Wang Z, Bi S, Song D, et al. Aldose reductase regulates miR-200a-3p/141-3p to coordinate Keap1–Nrf2, Tgfβ1/2, and Zeb1/2 signaling in renal mesangial cells and the renal cortex of diabetic mice. *Free Radic Biol Med.* 2014;67:91–102.
56. Iso K, Tada H, Kuboki K, Inokuchi T. Long-term effect of epalrestat, an aldose reductase inhibitor, on the development of incipient diabetic nephropathy in Type 2 diabetic patients. *J Diabetes Complications.* 2001;15:241–4.
57. Zhang ZH, Wei F, Vaziri ND, Cheng XL, Bai X, Lin RC, et al. Metabolomics insights into chronic kidney disease and modulatory effect of rhubarb against tubulointerstitial fibrosis. *Sci Rep.* 2015;5:14472.
58. Newgard Christopher B. Interplay between lipids and branched-chain amino acids in development of insulin resistance. *Cell Metab.* 2012;15:606–14.
59. Kumar MA, Bittla ARR, Raju KVN, Manohar SM, Kumar VS, Narasimha SRPVL. Branched chain amino acid profile in early chronic kidney disease. *Saudi J Kidney Dis Transpl.* 2012;23:1202–7.
60. Cano NJM, Fouque D, Lervere XM. Application of branched-chain amino acids in human pathological states: renal failure. *J Nutr.* 2006;136:299S–307S.
61. Mi N, et al. Branched-chain amino acids attenuate early kidney injury in diabetic rats. *Biochem Biophys Res Commun.* 2015;466:240–6.
62. Men LH, Pi ZF, Zhou Y, Liu YY, Wei MY, Song FR, et al. Metabolomics insights into diabetes nephropathy and protective effects of Radix Scutellariae on rats using ultra-high performance liquid chromatography coupled with quadrupole time-of-flight mass spectrometry. *RSC Adv.* 2017;7:16494–504.
63. Wei T, Zhao L, Jia J, Xia H, Du Y, Lin Q, et al. Metabonomic analysis of potential biomarkers and drug targets involved in diabetic nephropathy mice. *Sci Rep.* 2015;5:11998.
64. Kopple JD. Phenylalanine and tyrosine metabolism in chronic kidney failure. *J Nutr.* 2007;137:1586S–1590S. discussion 97S–98S.
65. Itoh Y, Ezawa A, Kikuchi K, Tsuruta Y, Niwa T. Protein-bound uremic toxins in hemodialysis patients measured by liquid chromatography/tandem mass spectrometry and their effects on endothelial ROS production. *Anal Bioanal Chem.* 2012;403:1841–50.
66. Macdonald G, Assef R, Guiffre A, Lo E. Vasoconstrictor effects of uridine and its nucleotides and their inhibition by adenosine. *Clin Exp Pharmacol Physiol.* 1984;11:381–4.
67. Liu J, Wang C, Liu F, Lu Y, Cheng J. Metabonomics revealed xanthine oxidase-induced oxidative stress and inflammation in the pathogenesis of diabetic nephropathy. *Anal Bioanal Chem.* 2015;407:2569–79.